URSI-B EMTS 2025, Bologna, 23–27 June

Design of a Multifrequency and Multibeam Transmitarray Based on Dielectric Cells

Andrea Dalle Piagge *(1), Francesco Alessio Dicandia (2), Simone Genovesi (1)
(1) Dipartimento Ingegneria dell'informazione, University of Pisa
Via G. Caruso 16, 56122, Pisa, Italy
(2) Cnr-Istituto di Elettronica e di Ingegneria dell'Informazione e delle Telecomunicazioni, Pisa, Italy

Abstract

This paper presents the design of an innovative transmitarray (TA) capable of multifrequency operation and multibeam generation by exploiting dielectric cells. Traditional dielectric-based TAs often face challenges such as gain imbalance between beams and inconsistent phase responses across frequencies. The proposed solution overcomes these limitations by interleaving cells dedicated to different frequencies and employing the principle of superposition. Numerical simulations validate the proposed approach, demonstrating balanced gain among beams at multiple frequencies and achieving acceptable Peak Side Lobe Levels (PSLLs) despite the absence of any amplitude control. The obtained design exhibits the scalability and manufacturability of the described method, making it a promising component for applications in satellite communications, radar, and next-generation wireless systems.

1. Introduction

Transmitarray antennas have emerged as a versatile solution in modern wireless communication and sensing systems, combining the advantages of phased arrays and reflector antennas [1], [2], [3]. By offering high gain, beam-steering capabilities, and reduced complexity compared to fully active phased arrays [4], [5], [6], TAs are widely utilized in applications such as satellite communications, radar, and 5G networks [7], [8], [9]. The operating principle of TA relies on manipulating the phase of the transmitted wavefront through individual unit cells, which are typically arranged in a planar or quasi-planar structure. These unit cells introduce a specific phase shift, enabling beamforming, beam steering, or multibeam generation. However, traditional TAs based on dielectric cells face significant limitations. One of the primary challenges is maintaining consistent phase and amplitude responses across multiple frequencies. This inconsistency arises from the frequency-dependent behavior of dielectric materials, which affects both the phase shift and impedance matching. Additionally, traditional approaches often require complex multi-layer designs, increasing fabrication complexity and reducing scalability [10] [11]. To address these challenges, two innovative solutions are proposed in this paper. The former solution involves interleaving cells corresponding to different frequencies. Each cell is designed to independently manipulate the phase of the transmitted wavefront at its target frequency, ensuring multifrequency functionality. While this approach mitigates the limitations of traditional designs and simplifies manufacturability, it exhibits gain imbalances when multiple beams are generated simultaneously. The latter one builds upon the interleaved configuration by incorporating the principle of superposition. In our work, a single cell is responsible for generating beams at different frequencies. This additional feature not only balances the gain across beams but also enables the creation of heterogeneous beam configurations, such as generating multiple beams at one frequency and fewer beams at another, without altering the overall structure.

2. Design of multifrequency and multibeam transmitarray

The design of the TA macro-cell has been developed using an innovative approach involving the interleaving of units dedicated to different operating frequencies. This technique optimizes the system's multifrequency performance, improving the consistency of phase and amplitude responses across all target bands. Two solutions have been proposed for arranging the interleaved units, each offering specific advantages in terms of performance and fabrication complexity. The solutions are illustrated in Figure 1 and described below.

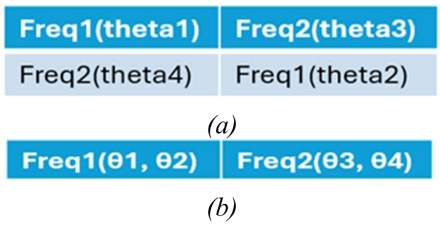

Figure 1. *(a)* Interleaved approach where each of the 4 cells is dedicated to one of the two frequencies and a pointing direction. *(b)* Interleaved approach and superposition principle**.**

The solution in Figure 1(a) assigns a pointing direction to each of the four cells at a specific frequency. However, this one has limitations when attempting to increase the number of beams of the TA, as this would require changing the structure's geometry. On the other hand, the solution in Figure 1(b) also utilizes the principle of superposition, where a single cell is responsible for generating both beams for a given frequency. The advantage of this solution is that the structure of the macro-cell does not need to be modified if the number of beams is increased. In Figure 2 we see the TA geometry.

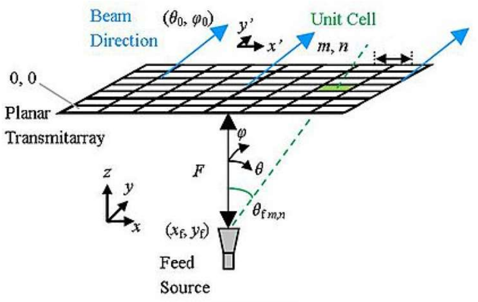

Figure 2. TA geometry.

3. Numerical assessment

A: *Microcell with interleaved approach*
First, the two TAs were simulated for the two frequencies and different pointing directions independently, with a cell count of 80x80. The chosen frequencies are 10 GHz and 15°GHz. A periodicity of λ/4 was selected, using the smaller wavelength between the two frequencies to avoid grating lobes. The TA is illuminated by an ideal point-source feeder characterized by a radiation pattern shape equal to $\cos(\theta)^{1.5}$ with an F/D parameter set to 0.35. F is the focal length, which represents the distance between the focal point (where the feeder or illuminator is positioned) and the center of the TA and D is the diameter of the TA. After obtaining the two solutions for the two frequencies, the cells were then selected according to the scheme in Figure 1(a). When synthesizing a cell for a specific frequency, with the length of each cell fixed at 3 cm, the permittivity required for the transmission line can be derived by inverting the equation (1).

$$\Phi + 2k\pi = \frac{2\pi\sqrt{\varepsilon_r}d}{\lambda} \quad k = 1, \dots 10 \tag{1}$$

with d length of the transmission line, λ wavelength in air and Φ phase realized by the cell. This provides a set of permittivity values (ε_r) that the transmission line must achieve to produce the desired phase shift. This approach also allows an evaluation of how the cell performs at the other frequency. The implemented algorithm selects permittivity values from the available set that fall within the range of 1.5 to 15, as these are physically realizable by the 3D printer [12]. Among these, it chooses the value that minimizes the error between the phase (obtained at the other frequency) and the phase calculated as βd, ensuring the error is less than 0.0001. If no value meets this criterion, the algorithm randomly selects a value from the available set within the 1.5 to 15 range. Figure 3, Figure 4 and Figure 5 show the results of simulations.

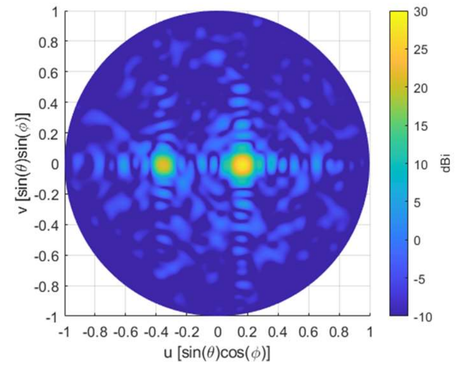

Figure 3. Representation of the gain in the *uv* plane at *freq1* = 10 GHz *(interleaved approach)*.

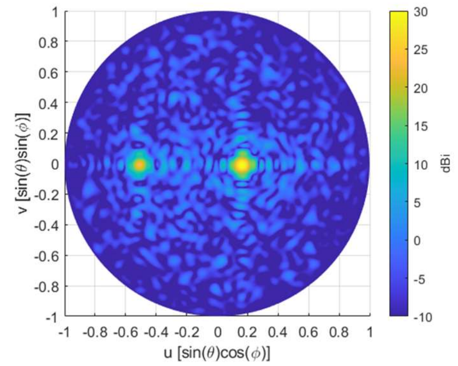

Figure 4. Representation of the gain in the *uv* plane at *freq2* = 15 GHz *(interleaved approach)*.

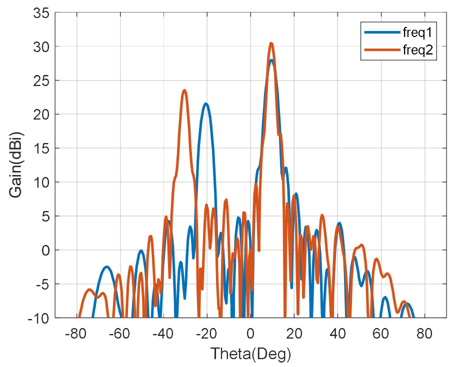

Figure 5. Gain section ($\Phi = 0°$).

B: *Microcell with interleaved approach and Superposition*
In the case where the cells are synthesized as shown in Figure 1(b), it is necessary to distinguish between scenarios with or without control over the amplitude. When superposition occurs, the optimal pattern is achieved by also controlling the amplitude assigned to each cell. The cell size d is fixed at 3 cm, and the F/D ratio is 0.35. Starting with the case of superposition without amplitude control, the phase required for each cell was calculated using Equation (2). This was done by first designing two independent TAs for the two frequencies and then selecting the cells according to the scheme shown in Figure 1(b).

$$\Phi_{nm} = angle\left\{\sum_{b=1}^{B} e^{j\varphi_{nm,b}}\right\} \tag{2}$$

where B is the number of beams and n, and m index a specific cell.

The algorithm used to determine the permittivity of the line is the same as that employed in the previous case. Consequently, the values of ε_r are selected within the range of 1.5 to 15. The approach aims to minimize the initial impedance mismatch, between the air impedance and the transmission line impedance, allowing the phase introduced by the line to be reasonably approximated as βd [4]. Figure 6, Figure 7 and Figure 8 show the results of simulations.

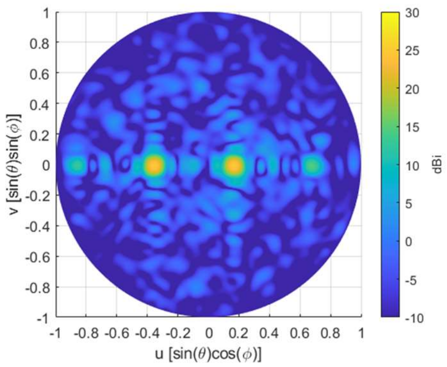

Figure 6. Representation of the gain in the *uv* plane at *freq1* = 10 GHz *(interleaved and superposition approach)*.

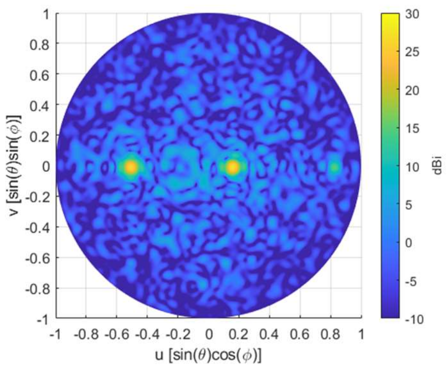

Figure 7. Representation of the gain in the *uv* plane at *freq2* = 15 GHz *(interleaved and superposition approach)*.

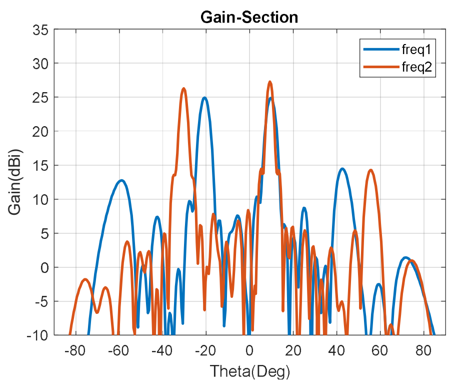

Figure 8. Gain section ($\Phi = 0°$).

Table 1. Comparison multifrequency with superposition.

	Freq1		**Freq2**	
Theta (deg)	-20	10	-30	10
Gain (dBi)	24.53	24.88	25.94	26.91
PSLL (dB)	-10.45		-12.85	

Table 2. Comparison multifrequency without superposition.

	Freq1		**Freq2**	
Theta (deg)	-20	10	-30	10
Gain (dBi)	21.18	27.97	23.40	30.35
PSLL (dB)	-15.89		-14.12	

Table 1 shows that, compared to the case without superposition, the two beams at the two frequencies are balanced, meaning they exhibit the same gain. This is not observed in the previous configuration (Table 2). Despite the lack of amplitude control, it is still possible to achieve reasonable PSLL values at both frequencies (
Table 1).

Another advantage of the superposition-based solution is its ability to generate more than two beams per frequency (Figure 9, Figure 10, Figure 11 and Table 3).

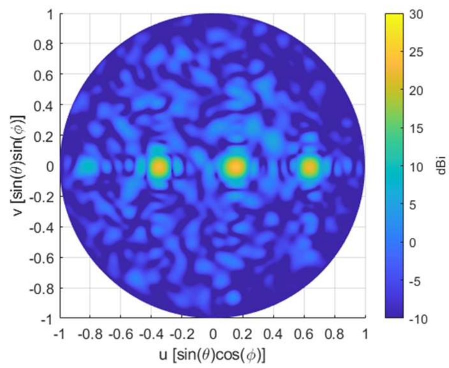

Figure 9. Representation of the gain in the *uv* plane at *freq1* = 10 GHz *(interleaved and superposition approach 3 beams)*.

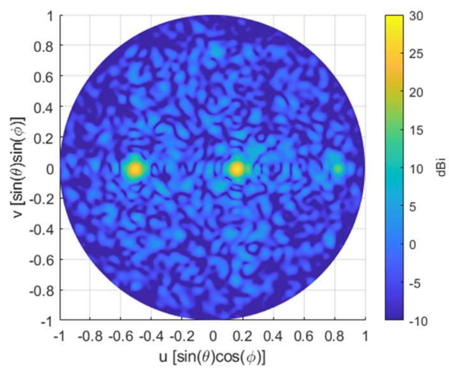

Figure 10. Representation of the gain in the *uv* plane at *freq2* = 15 GHz *(interleaved and superposition approach 2 beams)*.

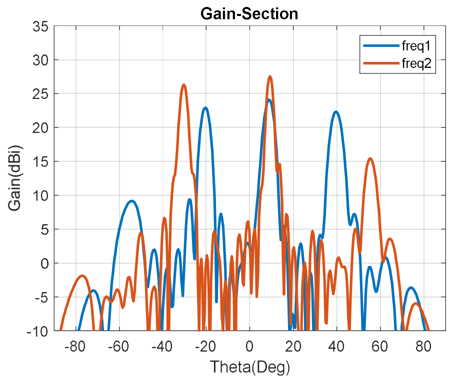

Figure 11. Gain section ($\Phi = 0°$).

Table 3. Comparison multifrequency with superposition heterogeneous beams.

	Freq1			Freq2	
Theta (deg)	-20	10	40	-30	10
Gain (dBi)	22.71	23.66	22.30	26.03	27.22
PSLL (dB)	-14.69			-12.24	

4.Conclusion

The design and analysis of multifrequency and multibeam TA using dielectric cells, with a focus on innovative interleaving and superposition techniques has been addressed. The results demonstrate that the proposed approach effectively balances the performance of beams at different frequencies, overcoming the gain imbalances observed in interleaving configuration only. The superposition-based solution not only simplifies the structural design but also enhances the system's flexibility, enabling the generation of multiple beams per frequency or heterogeneous configurations. Despite the absence of amplitude control, reasonable PSLL values were achieved, confirming the robustness of the proposed design methodology. Furthermore, the dielectric-based approach ensures scalability and manufacturability while maintaining high angular resolution and frequency stability. These findings highlight the potential of the proposed transmitarray design for applications in satellite communications, radar, and next-generation wireless systems

References

[1] J. R. Reis, M. Vala, and R. F. S. Caldeirinha, "Review Paper on Transmitarray Antennas," *IEEE Access*, vol. 7, pp. 94171–94188, 2019, doi: 10.1109/ACCESS.2019.2924293.

[2] F. A. Dicandia and S. Genovesi, "Characteristic Modes Analysis for Circularly Polarized 1-Bit Dual-Layer Transmitarray Design," *IEEE Open J. Antennas Propag.*, vol. 5, no. 1, pp. 112–123, Feb. 2024, doi: 10.1109/OJAP.2023.3340331.

[3] A. Clemente, L. Dussopt, R. Sauleau, P. Potier, and P. Pouliguen, "Focal Distance Reduction of Transmit-Array Antennas Using Multiple Feeds," *IEEE Antennas Wirel. Propag. Lett.*, vol. 11, pp. 1311–1314, 2012, doi: 10.1109/LAWP.2012.2227105.

[4] F. A. Dicandia and S. Genovesi, "Analysis of Performance Enhancement of Clustered-Based Phased Arrays Employing Mixed Antenna Element Factor," *IEEE Trans. Antennas Propag.*, vol. 72, no. 2, pp. 1439–1448, Feb. 2024, doi: 10.1109/TAP.2023.3340866.

[5] F. A. Dicandia and S. Genovesi, "Simultaneous Multibeam Clustered Phased Arrays Analysis Using Mixed and Multiple Antenna Element Factors," *Sensors*, vol. 24, no. 23, p. 7801, Dec. 2024, doi: 10.3390/s24237801.

[6] Y. Aslan, A. Roederer, N. Fonseca, P. Angeletti, and A. Yarovoy, "Orthogonal Versus Zero-Forced Beamforming in Multibeam Antenna Systems: Review and Challenges for Future Wireless Networks," *IEEE J. Microw.*, vol. 1, no. 4, pp. 879–901, Oct. 2021, doi: 10.1109/JMW.2021.3109244.

[7] M. J. Veljovic and A. K. Skrivervik, "Circularly Polarized Transmitarray Antenna for CubeSat Intersatellite Links in K-Band," *IEEE Antennas Wirel. Propag. Lett.*, vol. 19, no. 10, pp. 1749–1753, Oct. 2020, doi: 10.1109/LAWP.2020.3016340.

[8] F. A. Dicandia and S. Genovesi, "Low Profile Dual Linearly Polarized 1-bit Transmitarray Exploiting Two Metallic Layers," *IEEE Access*, vol. 12, pp. 56872–56879, 2024, doi: 10.1109/ACCESS.2024.3390775.

[9] L. Di Palma, A. Clemente, L. Dussopt, R. Sauleau, P. Potier, and P. Pouliguen, "Radiation Pattern Synthesis for Monopulse Radar Applications With a Reconfigurable Transmitarray Antenna," *IEEE Trans. Antennas Propag.*, vol. 64, no. 9, pp. 4148–4154, Sep. 2016, doi: 10.1109/TAP.2016.2586491.

[10] A. Massaccesi *et al.*, "3D-Printable Dielectric Transmitarray With Enhanced Bandwidth at Millimeter-Waves," *IEEE Access*, vol. 6, pp. 46407–46418, 2018, doi: 10.1109/ACCESS.2018.2865353.

[11] J. Lai, X. Lv, and Y. Yang, "A 3-D Printed 140 GHz Multifocal Dielectric Transmitarray Antenna for 2-D Mechanical Beam Scanning," *IEEE Antennas Wirel. Propag. Lett.*, vol. 23, no. 4, pp. 1366–1370, Apr. 2024, doi: 10.1109/LAWP.2024.3355940.

[12] F. A. Dicandia and S. Genovesi, "Mechanically Steerable Simultaneous Multibeam Transmitarray Design by Analytical Multifocal Approach," *IEEE Trans. Antennas Propag.*, vol. 72, no. 12, pp. 9129–9142, Dec. 2024, doi: 10.1109/TAP.2024.3485504.

[13] L. Liu *et al.*, "A Generalized Approach for Multifrequency Transmission Line Transformer With Frequency-Dependent Complex Source and Load," *IEEE Trans. Microw. Theory Tech.*, vol. 67, no. 9, pp. 3603–3616, Sep. 2019, doi: 10.1109/TMTT.2019.2926250.